Acta Materialia 235 (2022) 118096

Contents lists available at ScienceDirect

Acta Materialia

journal homepage: www.elsevier.com/locate/actamat

Full length article

Exploring domain continuity across $BaTiO_3$ grain boundaries: Theory meets experiment

Tamsin O'Reilly[a,b,*], Kristina Holsgrove[a], Ali Gholinia[c], Danielle Woodruff[d], Andrew Bell[d], John Huber[e], Miryam Arredondo[a]

[a] Centre for Nanostructured Media, School of Mathematics and Physics, Queen's University Belfast, United Kingdom
[b] University of Glasgow, United Kingdom
[c] Department of Materials, University of Manchester, United Kingdom
[d] School of Chemical and Process Engineering, University of Leeds, United Kingdom
[e] Department of Engineering Science, University of Oxford, United Kingdom

ARTICLE INFO

Article history:
Received 15 February 2022
Revised 4 May 2022
Accepted 9 June 2022
Available online 15 June 2022

Keywords:
Ferroelectrics
Ceramics
Domain compatibility
Electron microscopy
Domains

ABSTRACT

Polycrystalline ferroelectrics constitute the basis of many advanced technologies, including sensors and actuators. Their intricate domain patterns, and switching, drive the macroscopic electrical and mechanical properties of the material, where the domain switching behaviour is largely influenced by the grain-grain interaction of the domain walls. Domain wall continuity across grain boundaries is speculated to affect the domain wall – grain boundary interaction, although the true impact of this phenomenon on the ferroelectric properties, and the conditions under which continuity occurs, are not yet well understood. Whilst there are some theoretical reports, the link to experimental evidence is limited, greatly hindering the applicability and fundamental understanding of current polycrystalline based devices. In this work, we close this gap by studying several grain junctions in free-standing $BaTiO_3$ thin films using microscopy techniques and rationalising the domain configurations with reference to martensite theory. A pleasing agreement of minimal strain and polarisation mismatch for a pair of domain variants were found in cases where domain wall continuity across grain boundaries was observed, confirming that domain continuity is related to the compatibility conditions at the grain boundary. Following this experimental validation, the mismatches for various combinations of Euler angles in bi-grain junctions were theoretically explored, offering valuable insights into specific cases where domain continuity can be expected. These results offer an advancement in the understanding of grain-grain-domain interactions and provides a template for the prediction and control of domain wall continuity in polycrystalline ferroelectrics, appealing to those working in polycrystal design and domain engineering.

1. Introduction

Ferroelectrics are polar materials that possess a spontaneous polarisation (P_s) in the absence of an electric field. Their utility is derived from the ability to switch polarised domains by applying a sufficiently large external electric field, leading to polarisation hysteresis [1]. Domains are regions of uniform polarisation that form to minimise the electrical (ferroelectric) and often also the elastic (ferroelastic) energy present in the system, as the material is cooled from the paraelectric phase to below its Curie temperature (T_C). It is widely accepted that the arrangement, or pattern, of domains present, will greatly determine the macroscopic properties and the switching behaviour of the material [2–7]. For instance, it has been shown that the effective piezoelectric coefficients depend upon the fractions of different domain variants present [8], and enhanced actuation can be achieved by engineering specific domain patterns [3].

The formation of domains, in any ferroelectric, is mainly governed by three factors: the domain wall energy, the electrostatic energy, and the elastic energy. In a single crystal, the resulting domain configuration balances these energies, which are mainly dependant on the thickness of the crystal slab and the physical and electrical boundary conditions present [9,10]. However, most ferroelectrics used in today's sensors, actuators and electronic applications are polycrystalline, because of their low cost, fast preparation time scales and excellent electromechanical and dielectric properties [11]. Sintered ferroelectric ceramics comprise single-crystallite

* Corresponding author at: Queen's University Belfast, United Kingdom.
E-mail address: toreilly03@qub.ac.uk (T. O'Reilly).

https://doi.org/10.1016/j.actamat.2022.118096

grains of given size and random orientation, which are physically separated by grain boundaries (GBs). Each grain is mechanically constrained by its neighbours, inducing stress fields that extend from the GB into the grain [12,13]. Thus, additional to the factors above mentioned, the resulting domain configuration in a polycrystalline ferroelectric must balance long-range elastic and electrostatic interactions between grains of varying degrees of misorientation, when cooling through T_C. The domain patterns are influenced by the size [2,12–14] and orientation of the grains [15,16], the presence of GBs [15,17] and, to a lesser extent, other sintering factors such as the porosity [18]. Each will affect the domain switching and the global properties of these polycrystals. For example, the domain size has been shown to decrease with the square root of the grain diameter [13,14], with dielectric and piezoelectric measurements proving that domain wall motion decreases with decreasing grain size [19–21].

While doping is a route commonly used to tailor the switching properties of a ceramic material [22–24], crystallographic texture is another factor that can be used to enhance the ferroelectric properties, where GBs play a key role in domain formation and switching dynamics [25,26]. GBs are highly defective regions in the crystal structure, where the ferroelectric properties degrade, resulting in depolarising fields within the grains [17]. The switching process itself is a complex collective response across all grains, meaning that the switching in one grain influences the switching in the next grain and so on [27,28]. During switching, the nucleation of new domains often occurs near the GBs, resulting in high stress fields, which then propagate into the grain interior [15]. In theory, the stress would decrease if the macroscopic polarisation distribution could be correlated across neighbouring grains, with the domains meeting at the GB with the same periodicity. This requires continuity of spontaneous polarisation, P_s, and spontaneous strain, ε_s. At first sight this may seem highly improbable, considering that domain walls themselves are confined to certain crystallographic planes and that untextured ceramics have randomly orientated grains. However, domain wall continuity across GBs appears to be relatively common, with experimental observations published in $BaTiO_3$ (BTO) [29] and $Pb[Zr_xTi_{1-x}]O_3$ (PZT) [30,31]. Where in some cases, the character of the grain boundary has been reported to play a significant role [25,31].

It is speculated that domain continuity affects GB-domain interactions and produces a coupling effect between grains, but there are still conflicting reports on whether domain continuity acts to inhibit or enhance the ferroelectric properties [13,25,32,33]. The most exciting possibility is that domain continuity would allow a collective switching response over several grains, meaning that the domain structure within one grain would change due to the switching of domains from neighbouring grains [12,34,35]. In this picture, those GBs that do not promote domain continuity could be considered as pinning sites, reducing the bulk polarisation during switching [36]. With this assumption, it is conceivable that textured ceramics and polycrystalline thin-films with a degree of domain continuity could offer excellent potential for smart novel devices. Therefore, it is of high scientific and technological importance to deepen our understanding of this phenomenon.

There have been few efforts in the literature that directly investigate the theoretical conditions that allow domain wall continuity across GBs in polycrystalline ferroelectrics. Of note, the work of Mantri et al., who presented the mathematical requirements for domain wall plane matching between bi-grains in several crystal systems of BTO and linked this to the expected polarisation charge generated on the boundary itself, confirming a relationship between the domain pattern and the grain geometry [32,36]. On the experimental front, most efforts have been devoted to understanding the role of GBs in polycrystalline ferroelectrics by investigating the influence of single GBs on domain patterns and domain wall motion [25,26]. Previous studies on domain continuity in ceramic PZT found that the grain boundary character, based on coincident site lattice and plane-matching models, plays a significant role in domain continuity at the GBs [31]. However, the energetic contributions and conditions under which domain continuity will occur were not considered.

In this study, we investigate domain continuity across GBs in lamellae grain junctions cut from an un-doped $BaTiO_3$ (BTO) ceramic, by combining electron microscopy techniques and the theory of compatibility in terms of martensite crystallography adapted for free-standing polycrystalline films [37]. Typically, the notion is that the constraints on grains in bulk polycrystalline ferroelectrics are so severe that stress-free states are unlikely and complex energy minimising domain patterns form [38,39]. However, in polycrystalline thin films and free-standing lamellae, it is thought that the out-of-plane constraints can be relaxed, giving the material greater freedom to adopt a stress-free configuration [40], making these ideal candidates to study domain continuity. Firstly, a bi-grain sample, where the grains are of near identical orientation, was used to demonstrate the practical feasibility and provide a proof-of-concept for studying domain compatibility in free-standing thin films. This investigation was then extended to bi-grain junctions of higher misorientation, confirming that domain continuity can be predicted. Finally, we applied this method to a more representative example of a real polycrystalline sample, where multiple grains meet at a grain junction surrounding a pore. The presented method provides valuable insight into how domain compatibility methods can be used as a tool to explore and design microstructural arrangements with domain continuity in polycrystalline ferroelectrics and presents for the first time, a comprehensive experimental data set that analyses domain wall continuity.

2. Experimental methods

Scanning transmission electron microscopy (STEM) on a high-angle annular dark-field imaging (HAADF) detector was used to image 90° ferroelectric-ferroelastic domains, present within lamellae cut from a BTO ceramic (average grain size $\sim$ 25 μm). Unlike conventional TEM imaging, STEM-HAADF imaging provides less diffraction contrast and therefore allows a clearer identification of the 90° domains and the GB. It should be noted that STEM is less sensitive to 180° domain contrast. BTO is a well-studied ferroelectric, with a simple crystal structure and hence is suitable for this type of study. BTO powders were prepared by calcination of ball-milled $BaCO_3$ and TiO_2 at 1100 °C for 4 h. During the latter stages of a post-calcination ball mill, 2 wt% of a PVA binder was added. Green pellets 10 mm in diameter were prepared by uniaxial die pressing under a load of 10 tonne for 20 s. Prior to sintering, the pellets were heated at 50 °C/h and held at 550 °C for 4 h to burn out the binder. They were then heated at 300 °C/h to 1340 °C and held for 16 h before cooling to room temperature at a nominal 300 °C/h. The ceramic was polished using polishing papers and 50 nm colloidal silica. Secondary electron (SE) imaging provided clear visualisation of the grains, the GBs, and the domains, allowing regions of promoted domain continuity to be identified, see Fig. 1(a). Electron backscatter diffraction (EBSD) was carried out using an Oxford Nordlys detector on the bulk sample, see Fig. 1(b), and transmission kikuchi diffraction (TKD) was performed on the lamellae samples (30 kV, 6 nA) [41,42]. The EBSD patterns were indexed using the inbuilt Oxford Instruments AZtec software to obtain the orientation for each grain in Euler angles based on the Bunge convention. BTO has tetragonal crystal structure, with $a = b = 3.99\mathring{A}$ and $c = 4.03\mathring{A}$ [43], where tetragonality of the unit cell is very small. Therefore, the EBSD pattern indexing was simplified by assuming a cubic crystal symmetry with $a = 4.01\mathring{A}$ [44], to

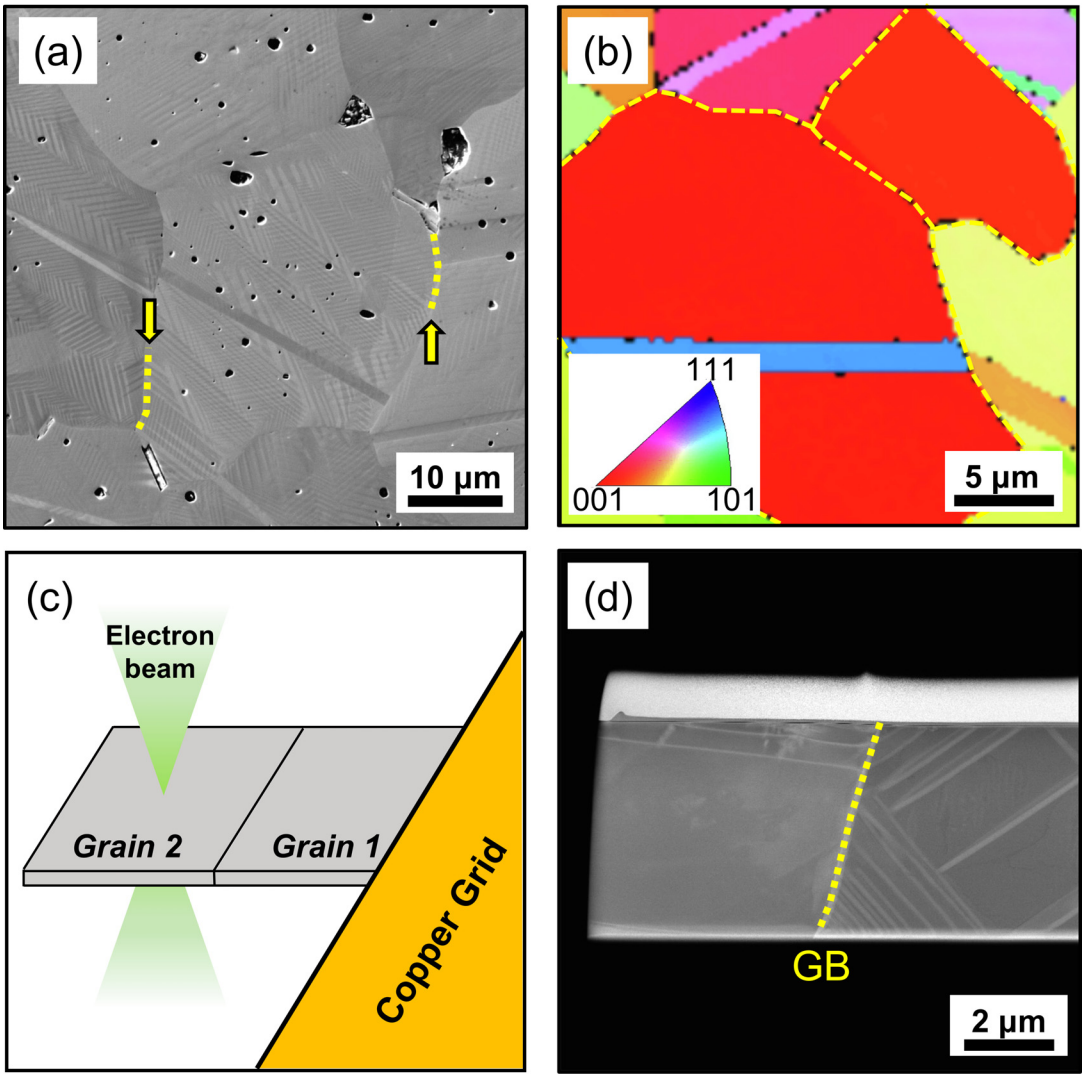

Fig. 1. Experimental set-up. (a) Secondary electron image of the polished ceramic. The yellow dotted lines indicate the GBs, and the yellow arrows depict regions along the GB where some degree of domain continuity is observed. (b) Representative inverse pole figure (IPF) map of the bulk sample using EBSD with a cubic solution. Orientation map shown in the inset. (c) Schematic representation of a bi-grain lamella on a Cu grid for STEM analysis. The electron beam is perpendicular to the sample surface in all cases. (d) Representative STEM-HAADF image of a bi-grain junction.

avoid pseudosymmetry issues, only identifying the grain orientations. The Euler angles were taken as an average from 5 high quality EBSD patterns from the TKD of each grain. Seven BTO lamellae sections were prepared in a TESCAN LYRA 3 dual beam SEM-focused ion beam microscope (SEM-FIB) at 30 kV. Next, the lamellae (~14 µm x 6 µm) were transferred *in situ* to Cu grids (Fig. 1(c)) and milled with ion beam currents (1 nA–50 pA), to the desired thickness (150–200 nm). Finally, 5 kV was used to polish the surface of the lamellae to improve surface quality. STEM-HAADF was performed on an FEI TALOS F200 G2 at 200 kV. The current was minimised (~50 pA) to prevent electron beam mediated domain nucleation while still allowing a good contrast between grains, grain boundaries and domains in the sample (Fig. 1(d)).

3. Electrical and mechanical compatibility

The total energy in a ferroelectric-ferroelastic system is largely the sum of the contributions from the domain wall energy, the electrostatic energy, and the elastic energy. Classical Landau-Ginzburg-Devonshire theory [45–47] predicts the presence of multiple energy wells in the crystal which correlates to different spontaneously polarised states, where energy minimisation results in the manifestation of domains [48]. Energy minimisation based on a multi-well theory (martensite theory), predicts that the domains in ferroelectric (and other ferroic) materials, will form characteristic patterns of low energy domain walls, which conform to simple electrical (electrostatic) and mechanical (elastic) compatibility conditions [38]. Domain walls with a low energy configuration are said to be compatible if they have no net charge (continuity of the normal component of electrical polarisation) and no dislocations (continuity of lattice strain) at the boundary [49]. For a pair of ferroelectric domains i and j with lattice strain states $\boldsymbol{\varepsilon}_i, \boldsymbol{\varepsilon}_j$, and corresponding polarisation vectors $\mathbf{p}_i$, $\mathbf{p}_j$, the interface normal vector $\mathbf{n}$ of a compatible domain wall must satisfy [38,48–51]

$$\boldsymbol{\varepsilon}_i - \boldsymbol{\varepsilon}_j = \frac{1}{2}(\mathbf{a} \otimes \mathbf{n} + \mathbf{n} \otimes \mathbf{a}) \tag{1}$$

$$(\mathbf{p}_i - \mathbf{p}_j) \cdot \mathbf{n} = 0 \tag{2}$$

Provided a vector $\mathbf{a}$ exists that satisfies Eq. (1), there is a compatibility of strains. Eq. (2) ensures continuity of electrical polarisation, giving a charge-free domain wall in the absence of external electric field or stress. It should be emphasised that Eqs. (1) and (2) are not necessary conditions for the formation of a domain

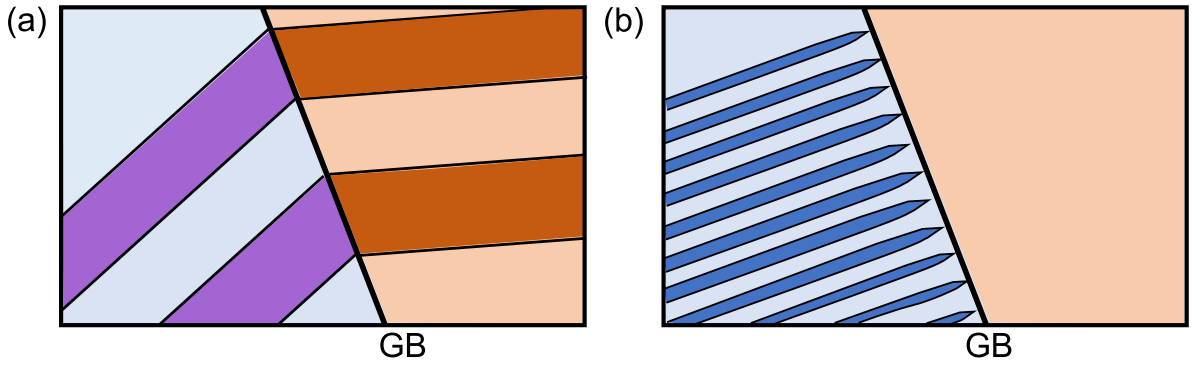

Fig. 2. (a) Domain wall continuity at a GB. The domain spacings and positions are matched. (b) No domain wall continuity. Fine needles may form to accommodate strain mismatch, large single domains may form preferentially on one side of the GB.

wall, but rather provide the conditions for an interface free of charge and dislocations. The consequences of these conditions have been considered in many ferroic material systems [38,48,49,51,52], and it has been established in experimental observations that domain walls do commonly form with the corresponding orientations that satisfy given compatibility conditions. In BTO, the six symmetric polarisation states take the form $\mathbf{p} = \pm P_0 \mathbf{e}_i$ $(i = 1 \cdots 3)$, where $\mathbf{e}_i$ are the orthogonal basis vectors of the tetragonal unit cell and P_0 is the spontaneous polarization magnitude. The corresponding strain states are given by

$$\boldsymbol{\varepsilon}_i = \varepsilon_0 \left(\frac{3\mathbf{p}_i \otimes \mathbf{p}_i}{2P_0^2} - \frac{1}{2}\mathbf{I} \right) \tag{3}$$

where ε_0 is the magnitude of the spontaneous lattice strain and $\mathbf{I}$ is the identity matrix. In the tetragonal system, compatible 180° domain walls can form in any plane parallel to any one of the $\mathbf{e}_i$ while compatible 90° domain walls only occur on ⟨110⟩ crystallographic planes.

Domain continuity between adjacent grains is defined to occur if the position and spacing of domains on one side of a GB is matched by corresponding domains on the other side of it Fig. 2(a)). This is more likely to arise when individual domains are compatible in pairs across the GB, and hence the matching spacing is expected to produce a low-energy arrangement of domains. At GBs, in addition to angular misorientation, there may also be linear translation of the lattice between adjacent grains. We were not able to detect this with the methods used in the present study. However, such translation would not cause strain or polarisation mismatch, and thus would only be associated with a surface energy term in the grain boundary energy. Where two domains in different grains meet at a GB with normal $\mathbf{n}_{gb}$, Eqs. (1) and ((2) may be applied to determine whether they form a low energy, compatible arrangement. If there is no such arrangement, alternative domain patterns that can reduce energy may form, and fine domains, with needle-like terminations at GBs, can be observed. These formations appear to reduce strain energy by satisfying compatibility in an average way, at the cost of increased domain wall energy (Fig. 2(b)).

In the context of GBs, it appears likely that the interface could contain dislocations and a space charge distribution. However, in the sintering process, crystals are bonded at high temperatures, above T_C (cubic phase); they then transform to ferroelectric phases upon cooling. Thus, the formation of domain patterns can accommodate strain compatibility and polarisation continuity at GBs if there are solutions to Eqs. (1) and (2). The strains $\boldsymbol{\varepsilon}_i, \boldsymbol{\varepsilon}_j$ now represent the lattice strains of particular domains in the different grains, and similarly $\mathbf{p}_i, \mathbf{p}_j$ are the corresponding spontaneous polarisation states. Since there may be an arbitrary rotation of crystal lattice between the grains, there is no guarantee of solutions to these equations, even if the symmetry related crystal variants in the individual grains can form compatible domain walls. It should be noted that other effects such as structural disorder, the presence of defects and potential differences in the local symmetry near the GB, which are factors that will likely affect domain continuity, are not considered here. It is the hypothesis of the current work that the appearance of continuity corresponds to the existence of solutions, or near misses, in Eqs. (1) and (2).

Mantri et al. [32,36] summarized the general conditions for continuity of a domain wall across a GB, including Eq. (2) and an additional condition on the domain wall orientations that allows them to meet at the GB (earlier given in the work of Fousek and others [53,54]), namely that

$$\mathbf{n}_{gb} \cdot \left(\mathbf{n}_i \times \mathbf{n}_j \right) = 0 \tag{4}$$

However, this treatment neglects the strain compatibility condition that is particularly significant in polycrystalline ferroelectrics due to the high elastic energy penalty associated with elastic mismatch, which originates from the grain misorientation. Here, we apply these conditions to specific experimental configurations in order to test the hypothesis that domain continuity is related to compatibility conditions across neighbouring grains in polycrystalline ferroelectrics. The experimental configuration tested is that of thin lamellae of BTO; this configuration provides additional freedom due to the free surfaces, and so makes the observation of compatible matches across GB more likely. In the lamella, it is expected that the constraint provided by Eq. (4) can be overcome by rotations of the domain wall out of its habit plane at the GB with minimal energy penalty. Similarly, mismatch in the out-of-plane strain components can be tolerated with minimal energy penalty due to the low thickness to size ratio. Furthermore, out-of-plane polarisation states are suppressed due to the requirement for charge compensation at the free surface. The special conditions in lamellar samples thus reduce the compatibility conditions to a simpler form. In particular, neglecting the out-of-plane strain components allows Eq. (1) to be rewritten as

$$\mathbf{t} \cdot \left(\boldsymbol{\varepsilon}_i - \boldsymbol{\varepsilon}_j \right) \cdot \mathbf{t} = 0 \tag{5}$$

where $\mathbf{t}$ is a unit vector parallel to the GB in the plane of the lamella, such that $\mathbf{t} \cdot \mathbf{n}_{gb} = 0$. If the polarisation vectors lie in the plane of the lamella, then, decomposing $\mathbf{p}_i$ as $\mathbf{p}_i = (\mathbf{p}_i \cdot \mathbf{n})\mathbf{n} + (\mathbf{p}_i \cdot \mathbf{t})\mathbf{t}$, expressing the tetragonal strain states in terms of polarisations through (3) and substituting into (5) shows that polarisation compatibility is implied by strain compatibility in this case. The conclusion is that in assessing the possibility of domain continuity across a GB in a thin lamella of tetragonal material, it is sufficient to test Eq. (5). If there are strain states that allow compatibility according to Eq. (5), continuity of polarisation is also possible.

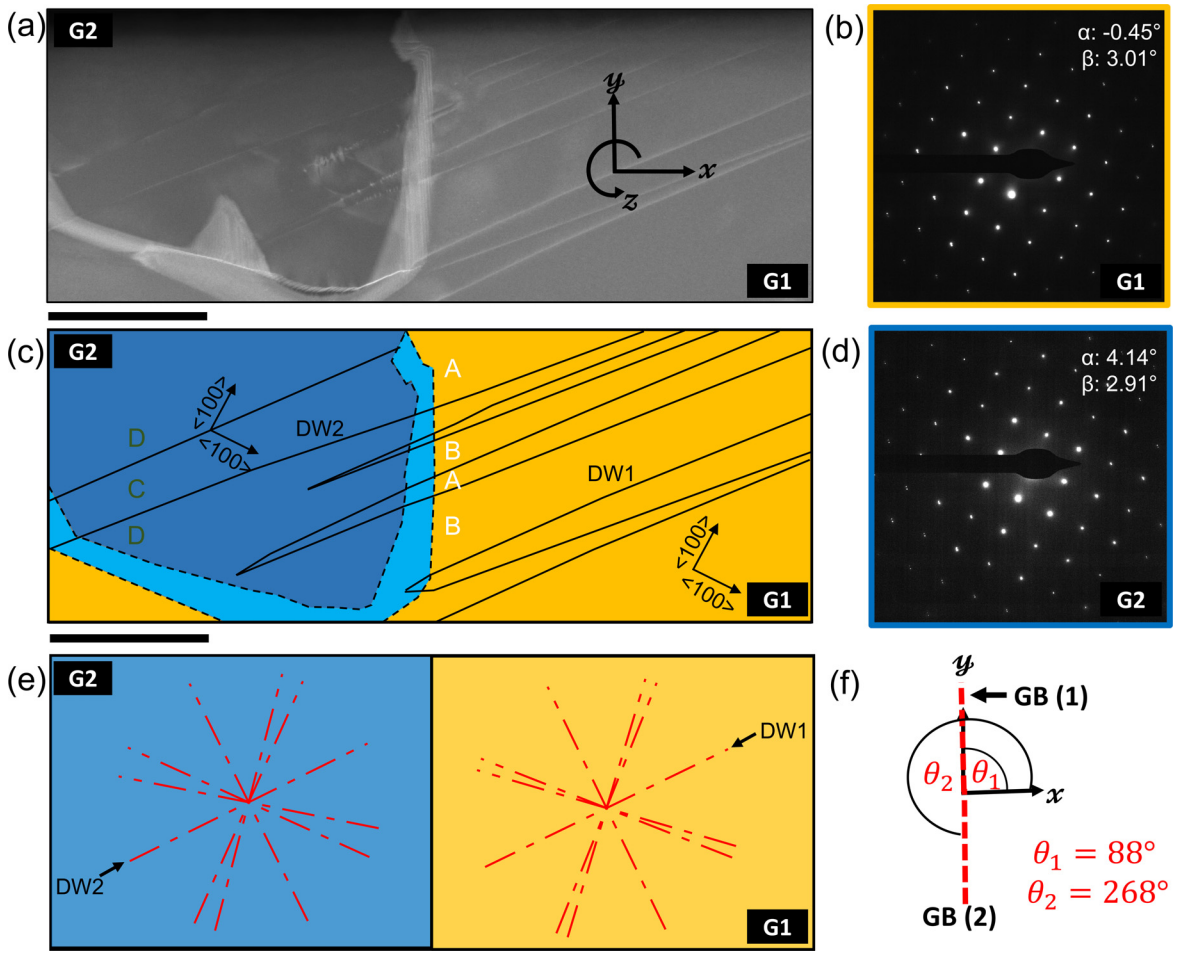

Fig. 3. Experimental observation of a bi-grain junction with small misorientation. (a) STEM image of a GB separating grains labelled G1 and G2, represented schematically in (c). The domains (labelled A-D) are orientated 45° from the local $<100>_{pc}$ axis, determined from the selected area electron diffraction (SAED) patterns for G1 (b) and G2 (d). The α and β values depict the tilt on the double tilt TEM holder required to orientate each grain 'on axis'. Schematic representation of (e) all permissible 90° walls for G1 and G2 are shown where domain wall 1 (DW1) from G1 and domain wall 2 (DW2) from G2 can be identified. The GB angles (f) between G1 and G2, GB (1), and G2 and G1, GB (2), are θ_1 and θ_2, respectively. The scale bar represents 1 µm.

3.1. Generating a proof-of-concept: inspecting a bi-grain junction of small misorientation

To generate a proof-of-concept for domain continuity across GBs, EBSD was employed to identify two grains closely orientated to each other, and to the $<100>_{pc}$ orientation (Fig. 1(b)). This served a dual purpose, (i) a degree of alignment between the grains was guaranteed, increasing the likelihood of domain continuity and (ii) the orientation guaranteed no projection effects at the domain boundaries, simplifying STEM analysis. The STEM-HAADF image in Fig. 3(a) confirms the first condition, clearly showing domains walls in grain 1 (G1, DW1) readily crossing into grain 2 (G2, DW2). To assess the compatibility of these domains, an area comprising the GB was taken. Fig. 3(c) is a schematic representation of the experimental STEM image from Fig. 3(a). The domain walls are orientated at 45° to the local $<100>_{pc}$ directions as determined from the diffraction patterns of each grain (Fig. 3(b) and (d)). This representation more clearly displays the 90° domains, labelled A-D, where domains A/C and B/D are continuous across the GB.

To rationalise the compatibility of the A/C and B/D domains using martensite theory, the transformation strains for each grain must be determined in global coordinates. The orientation of each grain in a polycrystalline system can be represented by three Euler angles (φ_1, ϕ, φ_2), in the Bunge convention. The Euler angles in the bi-grain shown in Fig. 3 were (115.4°, 3.6°, 45.5°) and (106.8°, 8.0°, 54.6°) for G1 and G2, respectively, giving a misorientation angle of 4.5°. The rotation matrix, $\mathbf{R}_i$, can be computed for each set of Euler angles, where the orientations of domain walls were then identified in each grain by using Eq. (1) to obtain the domain wall normal, $\mathbf{n}$, in local coordinates, where the domain walls are expected to appear in the STEM-HAADF images parallel to

$$\mathbf{e}_z \times (\mathbf{R}_i\mathbf{n}) \tag{6}$$

where $\mathbf{e}_z$ is the unit vector in the z-direction. This was incorporated into a MATLAB code[1] which draws and outputs all permissible $\{110\}_{pc}$ walls projected onto the plane of the lamella. By overlaying these walls onto the STEM image, Fig. 3(e), the contributing domain variants can be identified. For the case presented in Fig. 3, only two domain variants were present in each grain (A/B for G1 and C/D for G2), corresponding to the $(1\bar{1}0)$ wall in each grain. In total, 7 lamellae were studied, and in all cases the experimental domain walls in the STEM image matched within 2–3° of the theoretically permissible domain walls calculated from the $\mathbf{R}_i$. This was found to be an acceptable error, considering the challenging geometry required for TKD measurements. Upon further inspection, only (110) or $(1\bar{1}0)$ walls were found to be present experimentally.

[1] MATLAB code(s) are available on request. Please contact: john.huber@eng.ox.ac.uk

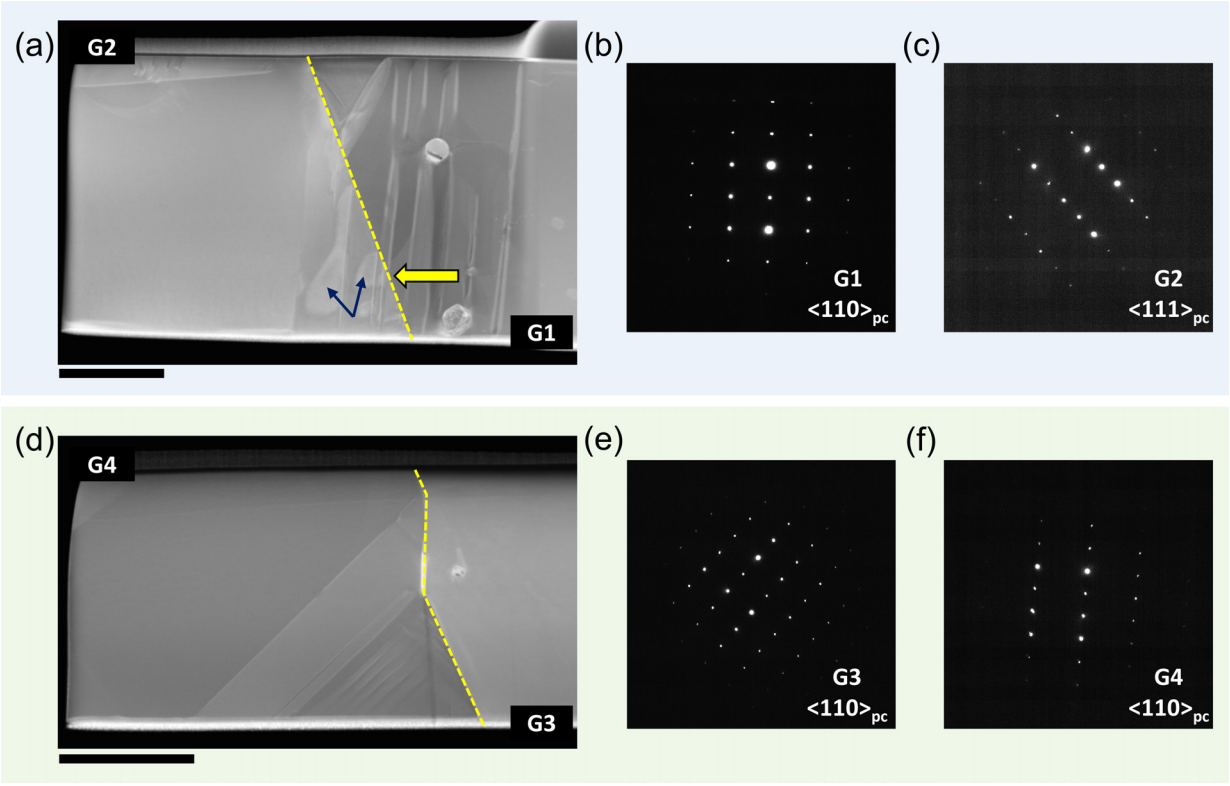

Fig. 4. Two bi-grain junctions with a high degree of misorientation between the grains. (a) A bi-grain sample that exhibits domain continuity and (d) a bi-grain sample that does not. In both cases the yellow dotted line indicates the GB. The large yellow arrow indicates where the domain continuity occurs in (a), with the small blue arrows highlighting the presence of 180° domains at the termination of the 90° needles due to the polarisation mismatch. The corresponding SAED for grains G1–G4 are shown in (b,c) and (e,f), respectively. Scale bar represents 2 μm.

This corresponds to the domain variants that have their polarisation lying approximately in the plane of the lamella. There are several potential explanations for the preference, which have already been touched upon at the start of Section 3. These are that (i) the lamellae is sufficiently thin, such that the out-of-plane compatibility conditions can be overcome with minimal energy cost and the intergranular constraints only form in-plane, (ii) mismatch in the out-of-plane strain components can be tolerated with minimal energy penalty due to the low thickness to size ratio and (iii) out-of-plane polarisation states may be suppressed due to the requirement for charge compensation at the free surfaces. It is likely that a combination of these factors results in the observed preference.

The GB angles were measured directly from the STEM image to be 88° between G1 and G2 (θ_1) and 268° between G2 and G1 (θ_2), when taken anticlockwise from the x-axis, see Fig. 3(f). It should be noted that the character of the GB (i.e., whether it is twist or tilt) has not been explicitly determined in this work. While interesting, a simplified approach considering the tangential and normal directions of the GB given by the GB angle, has proven to be sufficient to capture the general compatibility requirements for domain continuity to occur. The tangential direction, **t** and the normal direction, **n**, of each boundary are given by [cos(θ) sin (θ)] and [-sin(θ) cos (θ)], respectively.

After simplification of the problem to consider only the 'in-plane' strain variants present in each grain, the mismatch in the linear strain of domain A in G1 and domain C in G2 (l_{AC}) is then given by

$$l_{AC} = \mathbf{t} \cdot (\boldsymbol{\varepsilon}_A - \boldsymbol{\varepsilon}_C) \cdot \mathbf{t} \tag{7}$$

with similar calculations providing the mismatch for the other possible domain pairings. The strain mismatch is thus defined as the difference in linear stretch, relative to a reference cubic state, along the GB, normalized by the magnitude of the spontaneous strain, ε_s. Following this, the corresponding polarisation mismatch was calculated for each possible domain pair. The interfacial charge generated on the boundary by the domain pair can be considered in a similar manner to that reported by Mantri et al. [32,36], namely by considering the jump in the normal component of the polarisation. Between G1 and G2 where domains A and C meet, the polarisation mismatch (p_{AC}) is given by:

$$p_{AC} = ||\mathbf{P}_A \cdot \mathbf{n}| - |\mathbf{P}_C \cdot \mathbf{n}|\,|/P_0 \tag{8}$$

This is the minimum screening charge per unit area (normalised by P_0), required at the GB. We emphasise that Eq. (8) indicates that the polarisation mismatch at the boundary generates a charge at the interface and enables the minimum magnitude of charge per unit area to be calculated, as a fraction of the spontaneous polarisation, over the set of possible domain arrangements. Eq. (8) accounts for the uncertainty over the sign of polarisation in each strain variant, because there are two opposite polarisation states associated with each strain state. Similar calculations give the mismatch for the other possible domain pairings. In this example, the linear strain (l) and polarisation mismatch (p) between G1 variant 1 (V1) and G2 variant 1 (V1) was extremely low at $l = 0.006$ and $p = 0.004$. The values between G1 V2 and G2 V2 were similarly small at $l = -0.004$ and $p = 0.012$. Therefore, there exists two domain pairs with small mismatches, which can be continuous at the GB. In comparison, the other possible domain pairing resulted in significantly higher mismatches, and thus, these are unlikely to be continuous at the boundary. Given the sample symmetry, i.e., that $\theta_2 = \theta_1 + 180°$, the values for the second GB are identical and do not need to be reported. Further experimental details and full compatibility solutions for this bi-grain can be found in the supplementary material.

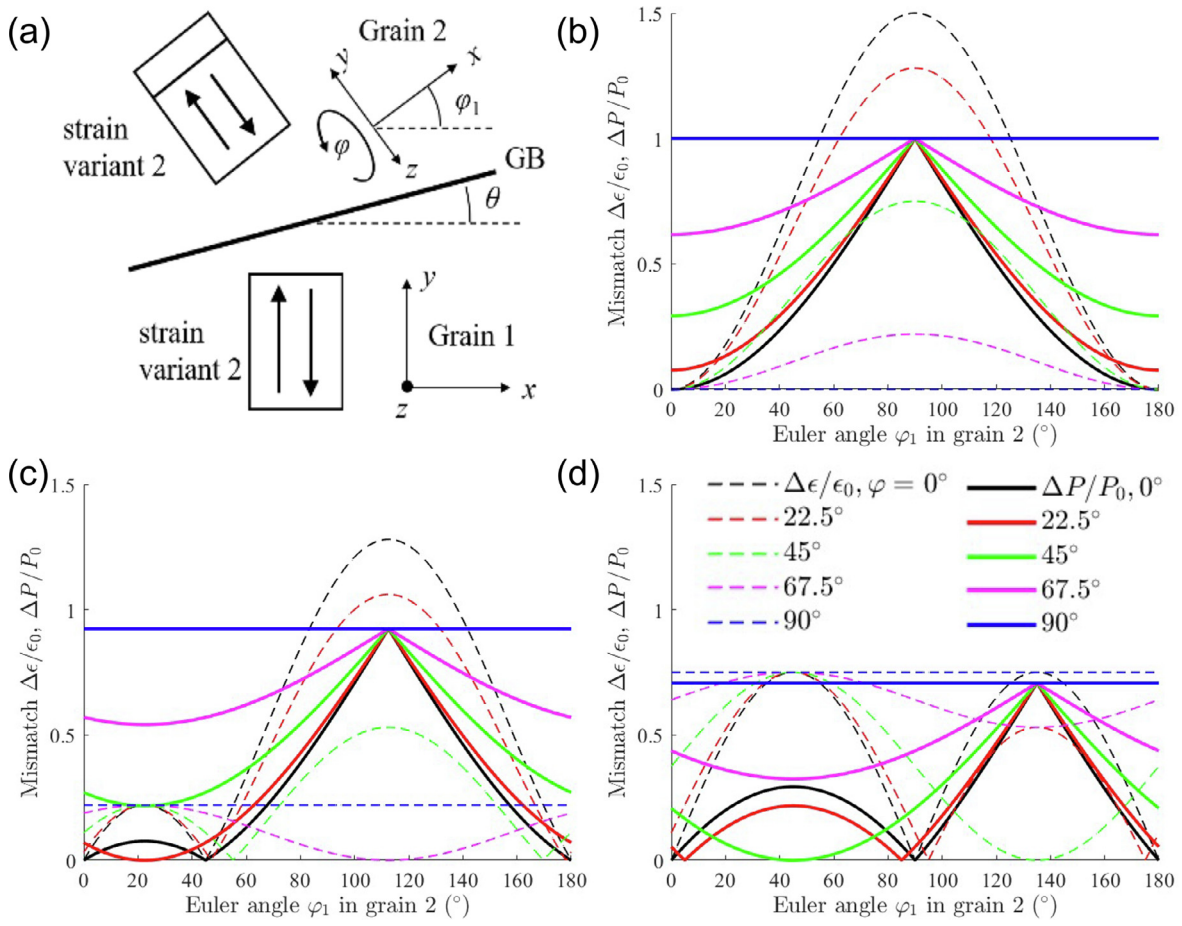

Fig. 5. Normalised strain and polarisation mismatches across a range of φ and φ_1 values. (a) Arrangement of domains adjacent to a GB in a lamella with three degrees of freedom indicated. (b-d) Strain and polarisation mismatches shown for various combinations of Euler angles in grain 2, with the GB angled (b) at 0°, (c) at 22.5°, and (d) at 45°

3.2. Investigating domain continuity in bi-grain samples of large misorientation

In Section 3.1, the small grain misorientation resulted expectedly in small mismatches at the GB. This situation is rare in untextured ceramics. In many cases, the mobility of the interfaces (GBs) are controlled by kinetic mechanisms, leading to metastable states that locally favour high-angle misorientations over low-angle values [55]. The question remains whether bi-grain junctions with large misorientation can form continuous, compatible domain arrangements at the boundary. Generally, high-angle GBs are described as having a misorientation greater than 15° [56]. Two experimental examples of such high-angle GBs are shown in Fig. 4. The resulting strain and polarisation mismatches for these junctions, and two additional examples, are fully reported in the supplementary material. For the first example (Fig. 4(a)–(c)), the experimental values are as follows:

- Grain 1 (G1) Euler angles – (100.9°, 43.2°, 33.3°)
- Grain 2 (G2) Euler angles – (127.4°, 35.2°, 8.7°)
- Misorientation between G1 and G2 – 18.8°
- Angle at GB (1), $\theta_1 = 113°$. Angle at GB (2), $\theta_2 = 293°$

In the second example (Fig. 4(d)–(f)), the experimental values are as follows:

- Grain 3 (G3) Euler angles – (218.9°, 28.6°, 18.0°)
- Grain 4 (G4) Euler angles – (245.2°, 18.5°, 25.3°)
- Misorientation between G3 and G4 – 34.6°
- Angle at GB (3), $\theta_3 = 90°$. Angle at GB (4), $\theta_4 = 293°$

Both examples were analysed following the methodology given in Sections 3.1 and 3. In the first example, Fig. 4(a), domain continuity is observed at the GB, indicated by the yellow arrow. This corresponds to the low mismatches between G1 V1 and G2 V1 ($l = -0.070$ and $p = 0.149$) and the other pair, G1 V2 and G2 V2 ($l = 0.070$ and $p = 0.034$). Interestingly, whilst the strain mismatch was of equal magnitude between the two pairs, the polarisation mismatch between these variants is significantly higher, implying a degree of mismatch. However, the system appears to compensate for this mismatch in the manifestation of 180° domains (marked by the blue arrows), close to the termination of the 90° domains in G2.

The compatibility of the in-plane domains were also assessed for the second example (Fig. 4(d)). There existed no pair of domain variants with low strain and polarisation mismatch in this case. Consequently, a more typical 90° pattern is adopted in G4 and G3 remains monodomain, similar to the case described in Fig. 2(b). Following observations of five bi-grain junctions and two tri-grain junctions, it was found that domain continuity generally occurs in cases where both the strain and polarisation mismatch between a pair of domain variants are < 0.3, see Fig. 7. Furthermore, testing the skewness of the experimental domain wall's intersection with the GB showed only coincidental matches between small error angles and cases of domain continuity, which confirmed that the constraint provided by Eq. (4) could easily be overcome due to the boundary conditions of the lamellae, see the supplementary

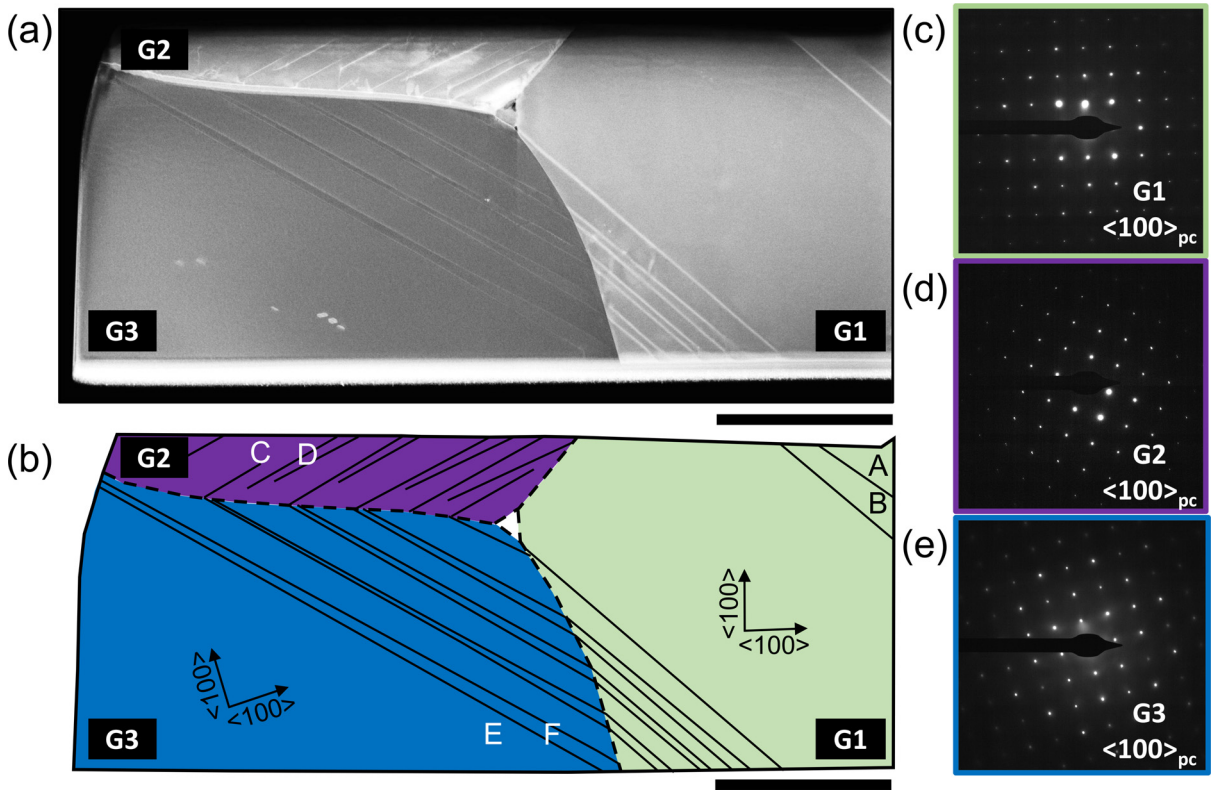

Fig. 6. Experimental observation of domain continuity occurring at a tri-grain junction surrounding a pore. (a) STEM image of the lamella, with grains labelled G1–G3, schematically represented in (b). The third grain is on axis in the image. The domains (labelled A–F) are orientated at 45° from the local $<100>_{pc}$ axis, determined from the SAED patterns (c–e). The scale bar represents 2 μm.

material for more information. Another factor to consider is the possibility that the domain wall can twist close to the GB, providing the match required by Eq. (4). In this configuration, this would be a low energy adjustment that might be observed as an apparent widening or narrowing of the projected image of the domain wall as observed by STEM.

3.3. Discussion of compatibility theory in bi-grain samples

Considering the good agreement between the compatibility framework and the experimental bi-grain junctions here investigated, the discussion was extended to cover theoretical arrangements in order to predict those orientations that will allow for domain continuity. As mentioned before, domain continuity across a GB is associated with elastic and electrostatic energies that depend upon the degree of mismatch in strain and polarisation, respectively. Based on Eq. (5) a strain mismatch can be calculated by:

$$\Delta\varepsilon = \left|\mathbf{t}\cdot\left(\boldsymbol{\varepsilon}_i - \boldsymbol{\varepsilon}_j\right)\cdot\mathbf{t}\right| \tag{9}$$

which is the magnitude of the difference in linear strain due to transformation from a reference cubic state for the two variants meeting at the GB. This calculates only the direct strain component along the GB, in the plane of the lamella. For the tetragonal crystal variants, $\Delta\varepsilon$ has maximum magnitude $3\varepsilon_0/2$. Similarly, the polarisation mismatch, based on Eq. (2) is

$$\Delta P = \min\left\{\left(\mathbf{p}_i \pm \mathbf{p}_j\right)\cdot\mathbf{n}_{gb}\right\} \tag{10}$$

which is a measure of the jump in polarisation normal to the GB. For tetragonal crystal variants the jump in polarisation has maximum magnitude $2P_0$. However, in practice values greater than P_0 are unlikely to be observed because in these cases it is always possible to replace one domain by an oppositely polarised domain and reduce the mismatch. Eq. (10) ensures that the minimum mismatch is chosen.

To illustrate the variation of $\Delta\varepsilon$ and ΔP in lamellae where two distinct domains meet across a GB, consider the simple arrangement in Fig. 5(a), representing a lamella situated in the *x*-*y* plane. Here, the global co-ordinate system is aligned with the crystal lattice of grain 1, wherein a domain polarized along the $\pm y$ axis meets the GB. Thus grain 1 has Euler angles (0,0,0) and the tetragonal strain variant present is variant 2. The GB is taken to be flat and normal to the surface of the lamella, orientated at angle θ to the *x*-axis. In grain 2, the Euler angles are $(\varphi_1, \varphi,\ 0)$ and variant 2 is again taken to be present. This restricts two of the five degrees of freedom associated with the GB (Euler angle φ_2 in grain 2 is fixed at zero, and the GB normal is forced to lie in the *x*-*y* plane). The resulting 3 degrees of freedom system is sufficient to illustrate the general idea of compatibility at the grain boundary.

Fig. 5(b)–d) show the normalised strain and polarisation mismatches $\Delta\varepsilon/\varepsilon_0$ and $\Delta P/P_0$ across a range of φ and φ_1 values, with separate results for GB angle $\theta = 0°,\ 22.5°$ and 45°. For the configuration shown in Fig. 5(b), $\theta = 0°$, the strain mismatch varies sinusoidally between zero and a maximum dependant on Euler angle φ. Similarly, the polarisation mismatch varies sinusoidally in the range $0° \le \varphi_1 \le 90°$ beyond which point the mismatch is minimised by switching the sign of polarisation, giving rise to symmetry about $\varphi_1 = 90°$. The sinusoidal variations are expected from simple rotation of rank 1 and rank 2 tensorial quantities. As the out-of-plane rotation φ varies, the dependence of polarisation mismatch on φ_1 reduces and the mismatch generally increases until, with $\varphi = 90°$ the polarisation mismatch is P_0 regardless of rotation φ_2 because the domain in grain 2 now has fully out-of-plane polarisation. When the GB orientation is $\theta = 22.5°$ or 45° (Fig. 5(c) and (d)) the dependence of strain and polarisation mismatch on the

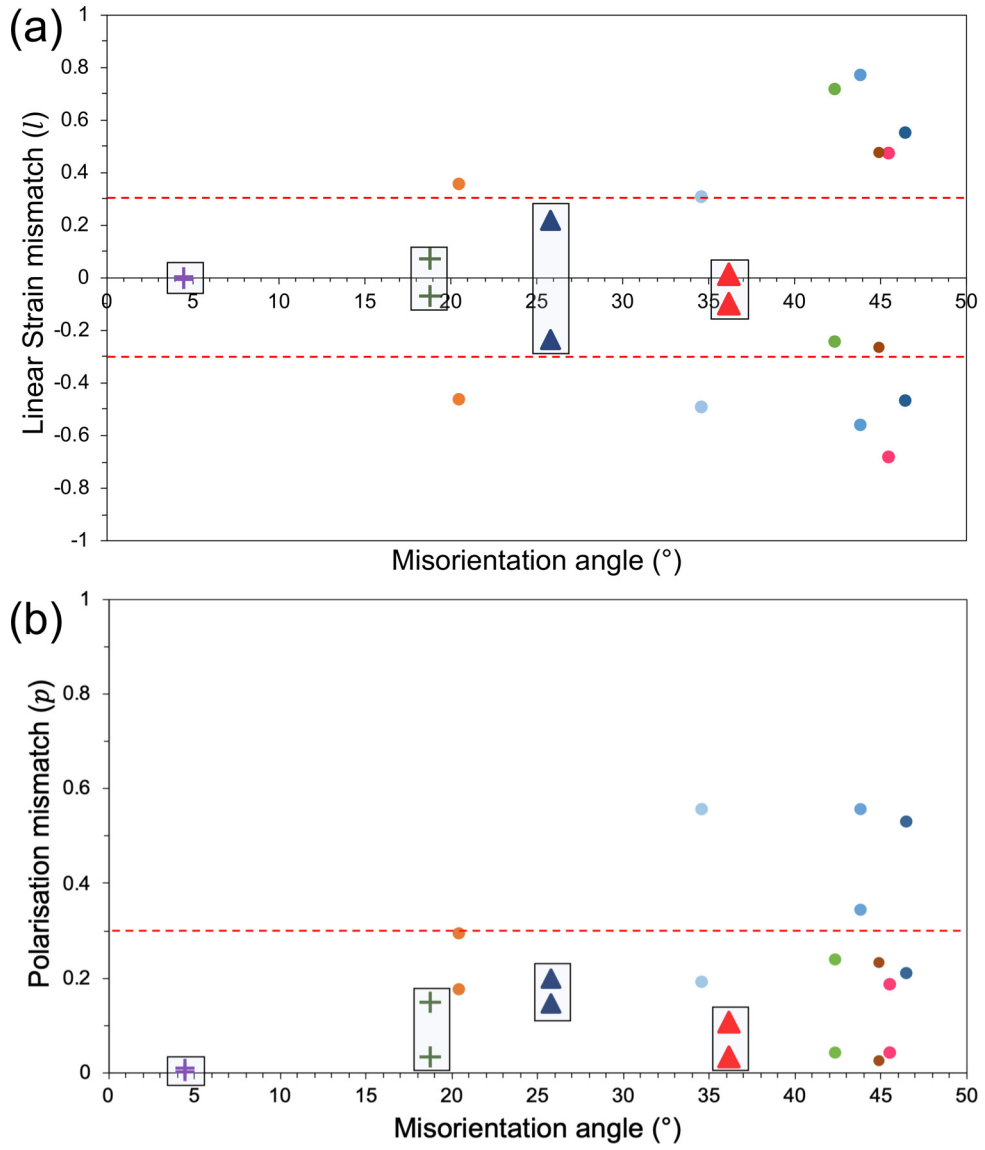

Fig. 7. Lowest calculated linear strain and polarisation mismatch for a pair of domain variants (2 data points) across 11 individual GBs of varying misorientation. (a) Linear strain mismatch (l) and (b) polarisation mismatch (p) vs. misorientation angle (°). Domain continuity is observed in four cases, where the normalised mismatches are < 0.3 for both l and p. Bi- and tri-grain samples that show domain continuity are represented by crosses and triangles, respectively, and highlighted by a box. All other boundaries that do not show domain continuity are shown as circles. The dotted red line indicates the cut-off value for both polarisation and strain mistmatch (< 0.3), above which domain continuity was no longer observed.

Euler angles of grain 2 has the same general character, but with shifted values. The symmetry about $\varphi_1 = 90^\circ$ is lost and discontinuities in slope occur wherever the underlying strain or polarisation values switch sign. The special case of $\theta = 45^\circ$ with $\varphi_1 = 90^\circ$ and $\varphi = 0^\circ$ is noteworthy: in this case the GB plays a role similar to that of a 90° domain wall, separating domain variants with orthogonal polarisation vectors, and the mismatches fall to zero.

A key observation from Fig. 5 is that conditions where polarisation compatibility is achieved do not generally correspond to conditions of strain compatibility. Thus, the use of one or other condition alone would not be sufficient to identify low energy continuous domain arrangements at a GB. However, in the special case of in-plane domains ($\varphi = 0^\circ$) strain mismatches of zero always correspond to polarisation mismatches of zero. Since most of the experimental observations considered in this paper concern in-plane, or nearly in-plane domains, there is typically a coincidence of near matches in strain and polarisation continuity. A further observation is that, although exact matching at the GB is rare, approximate matches (e.g. $\Delta\varepsilon/\varepsilon_0$ and $\Delta P/P_0$ both < 0.3) are common and can occur over a wide range of Euler angles.

3.4. Investigating domain continuity in a tri-grain junction

Bi-crystal configurations are often investigated because they offer a simple starting point for fundamental studies, both experimentally and theoretically [15,25,32,36]. However, bi-grain samples are not common in applications, nor do they resemble common cases found in polycrystalline materials. A more complex situation of interest is where multiple grains meet at a GB. An example of this is the tri-grain junction shown in Fig. 6. In this case, the situation becomes more interesting because there are 3 individual GBs and 6 experimentally present domain variants (labelled A–F) to consider. Each grain was determined to be closest to $<100>_{pc}$ from the SAED collected in each grain (Fig. 6(c)–(e)). The experimental data is as follows:

- Grain 1 (G1) Euler angles – (115.0°, 21.0°, 67.1°)

- Grain 2 (G2) Euler angles – (94.9°, 14.5°, 67.8°)
- Grain 3 (G3) Euler angles – (30.3°, 5.5°, 75.6°)
- Misorientation between G1 and G2 – 20.5°, G2 and G3 – 36.2° and G3 and G1 – 25.8°
- Angle at GB (1), $\theta_1 = 52^\circ$. Angle at GB (2), $\theta_2 = 176^\circ$. Angle at G3 (3), $\theta_3 = 300^\circ$.

The calculated strain and polarisation mismatches for each GB are fully reported in the supplementary material. There is no good compatibility agreement between G1 and G2, and the portion of G1 that shares the boundary with G2 does not form a domain pattern, remaining monodomain in similar fashion to the bi-grain junction from Fig. 4(d). Other regions of G1 does form domain walls. This is an interesting finding, demonstrating that portions of the same grain can form different domain structures depending on the associated strain and polarisation mismatch between domain pairs at the GB, which originates from the grain misorientation. Between G2 and G3, there existed a domain pair of low mismatch between G2 V1 and G3 V2 ($l = 0.012$ and $p = 0.107$) and the other pair G2 V2 and G3 V1 ($l = -0.100$ and $p = 0.035$). The system does attempt to create domain continuity, but some of the 90° domain walls terminated before they reached the boundary. It is plausible that this is due to large difference in the magnitude of the strain mismatch, which prevents full continuity. Between G3 and G1 the theory also predicted a pair of low mismatch variants between G3 V1 and G1 V2 ($l = 0.220$ and $p = 0.199$) and the other pair G3 V2 and G1 V1 ($l = -0.233$ and $p = 0.147$). In the lamella, the domains were readily continuous at the boundary. It should be noted that the reported strain and polarisation mismatch values of ∼0.23 and ∼0.22, respectively, were higher than any reported values from the bi-grain samples, see summary in Fig. 7. It is elucidated that the increased intergranular clamping and elastic constraint in the tri-grain junction allows for a higher tolerance of strain mismatch. The data for an additional tri-grain junction that does not exhibit domain wall continuity is shown in Fig. S8. At all three GBs, there existed no good compatibility agreement. In this case, where the domain structure formed at the GB in one grain, no domain structure formed at the same portion of the GB in the adjacent grain, in agreement with previous observations from all samples here investigated. The general observations of domain continuity were consistent between the bi-grain and tri-grain samples, indicating the potential scalability of this approach to predict domain configurations in more complex grain junctions. This is an important finding, which suggests that the results taken from free-standing thin films, can be incorporated into our understanding of the collective response of grains in polycrystalline materials, including thin films or bulk ceramics. However, it is expected that domain continuity in buried grains of ceramic materials will have much stricter compatibility constraints, due to 3D intergranular clamping.

3.5. Summary of results

In total, eleven individual grain boundaries, ranging from very small ($< 5^\circ$) to very large ($> 45^\circ$) misorientation between the adjacent grains were experimentally studied. In each case, the linear strain (l) and polarisation (p) mismatch were calculated for the possible domain pairings between the four in-plane domain variants (all values reported in the supplementary material). A plot of the misorientation angle vs. the calculated l and p values for the lowest mismatch pairing, representing the pairing most likely to allow domain continuity at the GB, are shown in Fig. 7. Each angular misorientation (GB) is represented in a different colour, where the four observed cases of domain continuity in the bi- and tri-grain junctions are represented by crosses and triangles, respectively, and highlighted for clarity. From this graph, it can be seen that polarisation and strain matching can occur over a large range of angular misorientations, in agreement with theoretical computations (Fig. 5). Importantly, the combined results from all the GBs indicate that the use of just one or other condition (l and p) alone is not sufficient to predict domain continuity. In fact, domain continuity was only found to occur in cases where mismatches were both < 0.3, marked as a cut-off value by the dotted red lines in Fig. 7. However, it is elucidated that the elastic mismatch provides the more significant contribution, considering that in all cases where $l < 0.3$, there is a coincidental match where $p < 0.3$, but the converse is not true. In this manner, it is confirmed that continuous domain structures can be predicted by compatibility conditions, directly relating to the system's ability to compensate the electrostatic and elastic charge generated by the strain and polarisation mismatch formed between two domain variants from adjacent grains which meet at the GB. It should be noted that the value of 0.3 may not be valid for other systems with greater spontaneous strain and matrix permittivity. It is hypothesised that a system with greater spontaneous strain will require a better alignment of the domain walls to lower the elastic energy at the GB, such that the tolerance value that allows domain continuity will decrease. Furthermore, additional contributions such as structural disorder, defects, changes in local symmetry, diffusion and presence of dopants near the GB, which have not been considered in this case, would likely affect domain continuity.

4. Conclusions

We have combined compatibility theory with electron microscopy techniques to investigate domain continuity in multiple free-standing thin films of BTO lamellae grain junctions, and established the following correlations between strain, polarisation and domain continuity across GBs: (i) domain continuity can be expected to occur when the calculated strain and polarisation mismatches between a pair of domain variants are **both** < 0.3. Domain continuity can therefore be related to, and predicted by, simple compatibility conditions, where the stability is largely determined by the magnitude of the electric and electrostatic charge generated at the boundary, and the ability of the material to screen the strain and polarisation mismatch. Importantly, we established that the use of one or the other condition alone is not sufficient to predict continuous domain arrangements. However, it was noted that there is typically a coincidence between low strain and low polarisation mismatch, indicating that the former mismatch makes a more considerable contribution in this configuration. (ii) When there exists no pair of variants with low strain and polarisation mismatch < 0.3 at a GB, the boundary is expected to be dominated by one good match on both sides of the boundary. Experimentally this resulted in little to no continuity. It was found that one grain would form a richer microstructure, whilst the other remained monodomain. (iii) It is predicted that if there are no good matches, the boundary is likely to have fine domains that minimise the energy by "average" compatibility. Following experimental validation, the discussion was extended to cover theoretical arrangements of bi-grain junctions, using the consideration that domain continuation can occur when $\Delta\varepsilon/\varepsilon_0$ and $\Delta P/P_0$ are both < 0.3. It was found that, whilst exact matching was rare, approximate matches were common and could occur over a wide range of Euler angles. Importantly, the results within this study offer a significant advance in the understanding of domain continuity at GBs, driven by both theoretical and experimental observations. This study appeals to those working in polycrystalline ferroelectrics, by identifying the conditions needed to promote or inhibit domain wall continuity, allowing more control over the ferroelectric properties. Furthermore, this work motivates exploration, by similar combination of experimental and theoretical work, of other technologically rel-

evant polycrystalline materials such as PZT. Of particular interest is how additional effects, such as the presence of doping agents and the occurrence of local symmetry breaking near the GB, as well as the magnitude of spontaneous strain and matrix permittivity, will affect domain continuity.

Declaration of Competing Interest

The authors declare that they have no known competing financial interests or personal relationships that could have appeared to influence the work reported in this paper.

Acknowledgments

This work was supported by the Engineering and Physical Research Council (Grant number EP/L015323/1). We would like to thank Dr. Josh Sugar for valuable TKD advice.

Supplementary materials

Supplementary material associated with this article can be found, in the online version, at doi:10.1016/j.actamat.2022.118096.

References

[1] G. Catalan, J. Seidel, R. Ramesh, J.F. Scott, Domain wall nanoelectronics, Rev. Mod. Phys. 84 (1) (2012) 119–156.
[2] G. Arlt, The influence of microstructure on the properties of ferroelectric ceramics, Ferroelectrics 104 (1990) 217–227.
[3] G.J. Weng, D.T. Wong, Thermodynamic driving force in ferroelectric crystals with a rank-2 laminated domain pattern, and a study of enhanced electrostriction, J. Mech. Phys. Solids 57 (3) (2009) 571–597.
[4] N. Liu, Y. Su, G.J. Weng, A phase-field study on the hysteresis behaviors and domain patterns of nanocrystalline ferroelectric polycrystals, J. Appl. Phys. 113 (20) (2013) 204106.
[5] S.E. Park, S. Wada, L.E. Cross, T.R. Shrout, Crystallographically engineered $BaTiO_3$ single crystals for high-performance piezoelectrics, J. Appl. Phys. 86 (5) (1999) 2746–2750.
[6] S. Wada, K. Muraoka, H. Kakemoto, T. Tsurumi, H. Kumagai, Preparation of potassium niobate crystals with fine engineered domain configurations and their enhanced piezoelectric properties, Ferroelectrics 319 (1) (2005) 127–134.
[7] J. Yin, W. Cao, Effective macroscopic symmetries and materials properties of multidomain $0.955Pb(Zn_{1/3}Nb_{2/3})O_3$-$0.045PbTiO_3$ single crystals, J. Appl. Phys. 92 (1) (2002) 444–448.
[8] J. Rödel, Effective intrinsic linear properties of laminar piezoelectric composites and simple ferroelectric domain structures, Mech. Mater. 39 (4) (2007) 302–325.
[9] Z. Chen, F. Li, Q. Huang, F. Liu, F. Wang, S.P. Ringer, H. Luo, S. Zhang, L.Q. Chen, X. Liao, Giant tuning of ferroelectricity in single crystals by thickness engineering, Sci. Adv. 6 (42) (2020) eabc7156.
[10] J.F. Ihlefeld, D.T. Harris, R. Keech, J.L. Jones, J.P. Maria, S. Trolier-McKinstry, Scaling effects in perovskite ferroelectrics: fundamental limits and process-structure-property relations, J. Am. Ceram. Soc. 99 (8) (2016) 2537–2557.
[11] J.Y. Li, R.C. Rogan, E. Ustundag, K. Bhattacharya, Domain switching in polycrystalline ferroelectric ceramics, Nat. Mater. 4 (10) (2005) 776–781.
[12] X.K. Li, J. Wang, Effect of grain size on the domain structures and electromechanical responses of ferroelectric polycrystal, Smart Mater. Struct. 26 (1) (2017) 015013.
[13] G. Arlt, P. Sasko, Domain configuration and equilibrium size of domains in $BaTiO_3$ ceramics, J. Appl. Phys. 51 (9) (1980) 4956–4960.
[14] W.W. Cao, C.A. Randall, Grain size and domain size relations in bulk ceramic ferroelectric materials, J. Phys. Chem. Solids 57 (10) (1996) 1499–1505.
[15] S. Choudhury, Y.L. Li, C. Krill, L.Q. Chen, Effect of grain orientation and grain size on ferroelectric domain switching and evolution: phase field simulations, Acta Mater. 55 (4) (2007) 1415–1426.
[16] S. Choudhury, Y.L. Li, C.E. Krill, L.Q. Chen, Phase-field simulation of polarization switching and domain evolution in ferroelectric polycrystals, Acta Mater. 53 (20) (2005) 5313–5321.
[17] W. Shu, J. Wang, T.Y. Zhang, Effect of grain boundary on the electromechanical response of ferroelectric polycrystals, J. Appl. Phys. 112 (6) (2012) 064108.
[18] H. Zhao, P. Wu, L. Du, H. Du, Effect of the nanopore on ferroelectric domain structures and switching properties, Comput. Mater. Sci. 148 (2018) 216–223.
[19] M. Demartin, D. Damjanovic, Dependence of the direct piezoelectric effect in coarse and fine grain barium titanate ceramics on dynamic and static pressure, Appl. Phys. Lett. 68 (21) (1996) 3046–3048.
[20] F. Griggio, S. Trolier-Mckinstry, Grain size dependence of properties in lead nickel niobate-lead zirconate titanate films, J. Appl. Phys. 107 (2) (2010) 024105.
[21] J.F. Ihlefeld, A.M. Vodnick, S.P. Baker, W.J. Borland, J.-P. Maria, Extrinsic scaling effects on the dielectric response of ferroelectric thin films, J. Appl. Phys. 103 (7) (2008) 074112.
[22] M.I. Morozov, D. Damjanovic, Hardening-softening transition in Fe-doped $Pb(Zr,Ti)O_3$ ceramics and evolution of the third harmonic of the polarization response, J. Appl. Phys. 104 (3) (2008) 034107.
[23] C. Wang, X. Yang, Z. Wang, C. He, X. Long, Investigation of switching behavior of acceptor-doped ferroelectric ceramics, Acta Mater. 170 (2019) 100–108.
[24] X. Gao, Z. Cheng, Z. Chen, Y. Liu, X. Meng, X. Zhang, J. Wang, Q. Guo, B. Li, H. Sun, Q. Gu, H. Hao, Q. Shen, J. Wu, X. Liao, S.P. Ringer, H. Liu, L. Zhang, W. Chen, F. Li, S. Zhang, The mechanism for the enhanced piezoelectricity in multi-elements doped $(K,Na)NbO_3$ ceramics, Nat. Commun. 12 (1) (2021) 881.
[25] D.M. Marincel, H. Zhang, A. Kumar, S. Jesse, S.V. Kalinin, W.M. Rainforth, I.M. Reaney, C.A. Randall, S. Trolier-Mckinstry, Influence of a single grain boundary on domain wall motion in ferroelectrics, Adv. Funct. Mater. 24 (10) (2014) 1409–1417.
[26] D.M. Marincel, H. Zhang, S. Jesse, A. Belianinov, M.B. Okatan, S.V. Kalinin, W.M. Rainforth, I.M. Reaney, C.A. Randall, S. Trolier-Mckinstry, Domain wall motion across various grain boundaries in ferroelectric thin films, J. Am. Ceram. Soc. 98 (6) (2015) 1848–1857.
[27] L.P. Tang, S.H. Xie, X.J. Zheng, Y.C. Zhou, J.Y. Li, Domain switching in ferroelectric ceramics beyond Taylor bound, Mech. Mater. 40 (4–5) (2008) 362–376.
[28] P. Bintachitt, S. Jesse, D. Damjanovic, Y. Han, I.M. Reaney, S. Trolier-Mckinstry, S.V. Kalinin, Collective dynamics underpins Rayleigh behaviour in disorded polycrystalline ferroelectrics, Proc. Natl. Acad. Sci. 107 (16) (2010) 7219–7224.
[29] G. Arlt, Twinning in ferroelectric and ferroelastic ceramics: stress relief, J. Mater. Sci. 25 (6) (1990) 2655–2666.
[30] A. Gruverman, O. Auciello, H. Tokumoto, Nanoscale investigation of fatigue effects in $Pb(Zr,Ti)O_3$ films, Appl. Phys. Lett. 69 (21) (1996) 3191–3193.
[31] S. Tsurekawa, K. Ibaraki, K. Kawahara, T. Watanabe, The continuity of ferroelectric domains at grain boundaries in lead zirconate titanate, Scr. Mater. 56 (7) (2007) 577–580.
[32] S. Mantri, J.E. Daniels, Ferroelectric domain continuity over grain boundaries for tetragonal, orthorhombic, and rhombohedral crystal symmetries, IEEE Trans. Ultrason. Ferroelectr. Freq. Control 65 (9) (2018) 1517–1524.
[33] D.M. Marincel, H.R. Zhang, S. Jesse, A. Belianinov, M.B. Okatan, S.V. Kalinin, W.M. Rainforth, I.M. Reaney, C.A. Randall, S. Trolier-McKinstry, Domain wall motion across various grain boundaries in ferroelectric thin films, J. Am. Ceram. Soc. 98 (6) (2015) 1848–1857.
[34] S. Wicks, K. Seal, S. Jesse, V. Anbusathaiah, S. Leach, R.E. Garcia, S.V. Kalinin, V. Nagarajan, Collective dynamics in nanostructured polycrystalline ferroelectric thin films using local time-resolved measurements and switching spectroscopy, Acta Mater. 58 (1) (2010) 67–75.
[35] Y. Jing, S. Leach, R.E. Garcia, J.E. Blendell, Correlated inter-grain switching in polycrystalline ferroelectric thin films, J. Appl. Phys. 116 (12) (2014) 124102.
[36] S. Mantri, J. Oddershede, D. Damjanovic, J.E. Daniels, Ferroelectric domain continuity over grain boundaries, Acta Mater. 128 (2017) 400–405.
[37] J.E. Huber, Micromechanics of ferroic functional materials, Advances in Nanocomposites, Springer, 2015.
[38] K. Bhattacharya, Microstructure of Martensite, Why it Forms and How it Gives Rise to the Shape-Memory Effect, Oxford University Press, Oxford, 2003.
[39] Y. Ivry, D.P. Chu, J.F. Scott, C. Durkan, Domains beyond the grain boundary, Adv. Funct. Mater. 21 (10) (2011) 1827–1832.
[40] Y.C. Shu, Heterogeneous thin films of martensitic materials, Arch. Ration. Mech. Anal. 153 (1) (2000) 39–90.
[41] A. Garner, A. Gholinia, P. Frankel, M. Gass, I. MacLaren, M. Preuss, The microstructure and microtexture of zirconium oxide films studied by transmission electron backscatter diffraction and automated crystal orientation mapping with transmission electron microscopy, Acta Mater. 80 (2014) 159–171.
[42] P.W. Trimby, Orientation mapping of nanostructured materials using transmission Kikuchi diffraction in the scanning electron microscope, Ultramicroscopy 120 (2012) 16–24.
[43] Y. Yoneda, Y. Kohmura, Y. Suzuki, S. Hamazaki, M. Takashige, X-ray diffraction topography on a $BaTiO_3$ crystal, J. Phys. Soc. Jpn. 73 (4) (2004) 1050–1053.
[44] R.H. Buttner, E.N. Maslen, Structural parameters and electron difference density in $BaTiO_3$, Acta Crystallogr. Sect. B Struct. Sci. 48 (1992) 764–769.
[45] A.F. Devonshire, Theory of ferroelectrics, Adv. Phys. 3 (10) (1954) 85–130.
[46] A.F. Devonshire, XCVI. Theory of barium titanate, Lond. Edinb. Dublin Philos. Mag. J. Sci. 40 (309) (1949) 1040–1063.
[47] A.F. Devonshire, CIX. Theory of barium titanate - part II, Lond. Edinb. Dublin Philos. Mag. J. Sci. 42 (333) (1951) 1065–1079.
[48] Y.C. Shu, K. Bhattacharya, Domain patterns and macroscopic behaviour of ferroelectric materials, Philos. Mag. B 81 (12) (2001) 2021–2054.
[49] N.T. Tsou, J.E. Huber, Compatible domain structures and the poling of single crystal ferroelectrics, Mech. Mater. 42 (7) (2010) 740–753.
[50] J.Y. Li, D. Liu, On ferroelectric crystals with engineered domain configurations, J. Mech. Phys. Solids 52 (8) (2004) 1719–1742.
[51] J.M. Ball, R.D. James, Fine phase mixtures as minimizers of energy, Arch. Ration. Mech. Anal. 100 (1) (1987) 13–52.
[52] A. Desimone, R.D. James, A constrained theory of magnetoelasticity, J. Mech. Phys. Solids 50 (2) (2002) 283–320.
[53] J. Fousek, P. Mokrý, Stress-free domain quadruplets in ferroics, Ferroelectrics 323 (1) (2005) 3–9.

[54] N.T. Tsou, P.R. Potnis, J.E. Huber, Classification of laminate domain patterns in ferroelectrics, Phys. Rev. B 83 (18) (2011).
[55] R.E. García, M.D. Vaudin, Correlations between the crystallographic texture and grain boundary character in polycrystalline materials, Acta Mater. 55 (17) (2007) 5728–5735.
[56] G. Faraji, H.S. Kim, H.T. Kashi, Effective parameters for the success of severe plastic deformation methods, in: Sever Plastic Deformation: Methods, Processing and Properties, Elsevier, 2018, pp. 187–222.